SCIENCE CHINA
Information Sciences

• RESEARCH PAPER •

July 2023, Vol. 66 172203:1–172203:18
https://doi.org/10.1007/s11432-022-3649-1

Fixed-time-synchronized control: a system-dimension-categorized approach

Wanyue JIANG[1], Shuzhi Sam GE[2] & Dongyu LI[3,4*]

[1]*Institute for Future & Shandong Key Laboratory of Industrial Control Technology, School of Automation, Qingdao University, Qingdao* 266071*, China;*
[2]*Department of Electrical and Computer Engineering, National University of Singapore, Singapore* 117576*, Singapore;*
[3]*School of Cyber Science and Technology, Beihang University, Beijing* 100191*, China;*
[4]*Shanghai Institute of Satellite Engineering, Shanghai* 201109*, China*

Received 23 July 2022/Revised 2 October 2022/Accepted 22 November 2022/Published online 17 May 2023

Abstract This study addresses the fixed-time-synchronized control problem of perturbed multi-input multi-output (MIMO) systems. In the task of fixed-time-synchronized control, different dimensions of the output signal in MIMO systems are required to reach the desired value simultaneously within a fixed time interval. The MIMO system is categorized into two cases: the input-dimension-dominant and the state-dimension-dominant cases. The classification is defined according to the dimension of system signals and, more importantly, the capability of converging at the same time. For each kind of MIMO system, sufficient Lyapunov conditions for fixed-time-synchronized convergence are explored, and the corresponding robust sliding mode controllers are designed. Moreover, perturbations are compensated using the super-twisting technique. The brake control of the vertical takeoff and landing aircraft is considered to verify the proposed method for the input-dimension-dominant case, which shows the essential advantages of decreasing the energy consumption and the output trajectory length. Furthermore, comparative numerical simulations are performed to show the semi-time-synchronized property for the state-dimension-dominant case.

Keywords fixed-time-synchronized convergence, sliding mode control, perturbed MIMO systems

Citation Jiang W Y, Ge S S, Li D Y. Fixed-time-synchronized control: a system-dimension-categorized approach. Sci China Inf Sci, 2023, 66(7): 172203, https://doi.org/10.1007/s11432-022-3649-1

1 Introduction

In practical applications, the temporal constraint is one of the most important requirements for a control system. Among the temporal-constraint-related control methods, fixed-time control has attracted considerable attention in recent years [1]. Extended from the well-known finite-time control which emphasizes the finite-time convergence [2,3], fixed-time control further requires global finite-time stability. Moreover, the bounded settling time in fixed-time control does not increase with the initial state [4]. The fixed-time control method has been used in many real-world applications, such as fault-tolerant control of robot manipulators [5], attitude tracking control of spacecraft [6], consensus control of multiagent systems [7, 8], and disturbance rejection control of wheeled mobile robots [9].

A Lyapunov condition is proposed in [10] as the basis for fixed-time stability. The terminal sliding mode technique is commonly used to meet the specific converging requirement of fixed-time control [11]. In affine systems and single-input single-output (SISO) systems, the terminal sliding mode surface can be designed to directly fit the Lyapunov condition and drive the system to fixed-time convergence [11, 12]. However, when we consider the fixed-time control of the multi-input multi-output (MIMO) system, challenges arise because of the necessary cooperation among different state dimensions. An elegant fixed-time controller should treat the MIMO system as a whole and drive all the state dimensions to the origin. Correspondingly, the terminal sliding mode surface should be extended to multiple dimensions and ensure the convergence of every dimension of the system output. Many explorations have been made

* Corresponding author (email: dongyuli@buaa.edu.cn)

to solve this problem, such as multivariable sliding mode control [13], sliding mode surface defined on the error vector [14], multidimensional sliding surface where each dimension works for different state components [15], and sign function that couples every state dimension [16].

In addition to the fixed-time control whose settling time depends on the slowest dimension of the output signal in MIMO systems, other temporal constraints may also be important. In some applications, time synchronization is required for the convergence of each output dimension. For example, all of the fingertips of a robotic hand should reach their desired angles at the same time when it tries to grasp a slippery object [17]. Time-synchronized convergence is expected in many cooperation tasks such as rendezvous of fixed-wing vehicles [18, 19], cooperative transportation by multiple vehicles [20], and saturation attack of multiple missiles [21]. In the authors' previous studies [22, 23], time-synchronized stability is defined and explored for relatively simple affine systems, whose output dimension matches its input dimension perfectly with no perturbations.

Motivated by this, the study focuses on the fixed-time-synchronized control of the MIMO system, in which each dimension of the output signal should converge simultaneously in a fixed time. Challenges exist in three aspects. Although many fixed-time control methods have been proposed, the integration of fixed-time control and time-synchronized convergence is under exploration for MIMO systems. The input and output dimensions of the MIMO system may not match each other, and whether the control input has enough capability to drive all output dimensions to achieve thorough fixed-time-synchronized convergence remains an open problem. The perturbations in the system further increase the difficulty of the controller design. The contributions of this study are outlined as follows.

First, the fixed-time-synchronized control problem is addressed. A series of Lyapunov conditions, which assure both fixed-time stability and time-synchronized convergence, are proposed to solve this problem. Fixed-time-synchronized controllers are designed based on the Lyapunov conditions, and the analysis of both the stability of the closed-loop system and the property of time-synchronization is conducted. In comparison with conventional fixed-time control methods [24, 25], the proposed method has the essential advantages of shorter output trajectory and lower energy consumption, all of which are particularly critical in the application of energy-sensitive vehicles [26].

Second, the capability of achieving fixed-time-synchronized convergence for the MIMO system, which is categorized into the input-dimension-dominant system (for thorough fixed-time-synchronized convergence that every output element converges simultaneously) and the state-dimension-dominant system (for semi-fixed-time-synchronized convergence that parts of output elements converge simultaneously), is explored. Different Lyapunov theorems are presented for each kind of MIMO system, which may provide the basis for time-synchronized control in more complicated cases.

Finally, perturbations in the system, which can be either matched disturbances or unmatched disturbances, are considered. To deal with perturbations, a multivariable super-twisting compensator is designed and embedded into the control system to ensure the achievement of fixed-time-synchronized convergence under disturbances.

In the rest of the paper, we introduce some technical preliminaries (Section 2), present the main results for input-dimension-dominant systems under matched and unmatched disturbances (Section 3), and extend it to the state-dimension-dominant case (Section 4). Simulations and comparative studies are conducted in Section 5, where the merit of the proposed approach is demonstrated. In Section 6, pertinent conclusions are finally drawn.

2 Preliminaries

Consider the following MIMO system:

$$\dot{x} = Ax + Bu + d(t, x, u), \tag{1}$$

where x, u, d are the system state, input, and disturbance, respectively. Let n be the dimension of x and m be the dimension of u. This paper focuses on the system with $1 \leqslant m \leqslant n$. The matrices A and B are with proper dimensions, and all perturbations are generally described by $d(t, x, u)$.

The first assumption we made is on system matrices.

Assumption 1. The system is controllable with matrices A and B. The matrix B has full rank and can be re-organized as $B = [B_1^{\mathrm{T}}, B_2^{\mathrm{T}}]^{\mathrm{T}}$, where $B_2 \in \mathbb{R}^{m\times m}$ and $\det(B_2) \neq 0$.

Inspired by the transformation method in [27–29], the general system (1) is transformed with

$$Tx = \begin{bmatrix} x_1 \\ x_2 \end{bmatrix},\ T = \begin{bmatrix} I_{n-m} & -B_1 B_2^{-1} \\ 0 & B_2^{-1} \end{bmatrix}, \tag{2}$$

and rewritten in a regular form,

$$\begin{aligned} &\dot{x}_1 = A_{11}x_1 + A_{12}x_2 + d_1(t,x), \\ &\dot{x}_2 = A_{21}x_1 + A_{22}x_2 + u + d_2(t,x,u), \\ &y = x_1, \end{aligned} \tag{3}$$

where $x = [x_1^{\mathrm{T}}, x_2^{\mathrm{T}}]^{\mathrm{T}}$ is re-organized in accordance with matrix B, $x_1 \in \mathbb{R}^{n-m}$ and $x_2 \in \mathbb{R}^m$ are system states, $y \in \mathbb{R}^{n-m}$ is the output, $d_1(t,x) \in \mathbb{R}^{n-m}$ can be regarded as the unmatched disturbance and $d_2(t,x,u) \in \mathbb{R}^m$ the matched disturbance, respectively. Hereinafter, we use d_1 and d_2 for short. The matrices A_{11}, A_{12}, A_{21}, and A_{22} are with proper dimensions.

The general system in (3) is defined as two categories.

Definition 1. The system (3) is called input-dimension-dominant if the input dimension (m) is not less than the output dimension ($n-m$), namely $m \geqslant \frac{n}{2}$, and called state-dimension-dominant otherwise.

Remark 1. When the output and input dimensions match each other and the system matrix has full rank in MIMO systems, it can be treated similarly to the affine system. However, practical systems can be less ideal. Over-actuation results in multiple solutions whereas under-actuation indicates the output components cannot be forced to converge at the same time. We categorize the MIMO system into the input-dimension-dominant case where the input has enough capability of driving the output to converge simultaneously, and the output-dimension-dominant case where the input is not capable of such an object.

Some definitions and lemmas are introduced on fixed-time control and time-synchronized stability.

Lemma 1 ([10])**.** A system with state x is fixed-time stable if there exists a function $V(x)$ such that $\dot{V}(x) \leqslant -(pV^{\alpha}(x) + gV^{\beta}(x))^k$ for positive $p, g, \alpha, \beta, k : k\alpha < 1, k\beta > 1$, and the settling time of the system can be written as $T(x_0) \leqslant (1/p^k(1-k\alpha)) + (1/g^k(k\beta - 1))$.

Definition 2 ([23])**.** System (1) is fixed-time-synchronized stable if (1) it is fixed-time stable, i.e., the bounded settling time $T(x_0) < T_m < \infty$, (2) the state elements converges time-synchronously, i.e., $x_i(t) \neq 0$ and $\lim_{t \to T(x_0)} x_i(t) = 0$ for $\forall t \leqslant T(x_0)$, and $x_i(t) = 0$ for $\forall t > T(x_0)$, where $T_m > 0$ is a constant.

Lemma 2 ([23])**.** The closed-loop state x of the system $f(x) = \dot{x}$ is ratio persistent if $x/\|x\| = \zeta f(x)/\|f(x)\|$ for $x \neq 0$ and $\zeta \in \{1, -1\}$.

Lemma 3 ([23])**.** The system state x is fixed-time-synchronized stable if it is fixed-time stable and the state x is ratio persistent.

A classical sign function in the existing literature is often defined as

$$\mathrm{sign_c}(x_i) \triangleq \begin{cases} +1, & x_i > 0, \\ 0, & x_i = 0, \\ -1, & x_i < 0, \end{cases} \tag{4}$$

with the following vector and exponential forms:

$$\mathrm{sign_c}(x) = [\mathrm{sign_c}(x_1), \ldots, \mathrm{sign_c}(x_n)]^{\mathrm{T}}, \tag{5}$$

$$\mathrm{sig_c^{\alpha}}(x) = [\mathrm{sign_c}(x_1)|x_1|^{\alpha}, \ldots, \mathrm{sign_c}(x_n)|x_n|^{\alpha}]^{\mathrm{T}}, \tag{6}$$

where $x = [x_1,\ x_2, \ldots,\ x_n]^{\mathrm{T}} \in \mathbb{R}^n$ is a state vector. In contrast, the norm-normalized sign function is

$$\mathrm{sign_n}(x) \triangleq \begin{cases} \frac{x}{\|x\|}, & x \neq 0, \\ 0, & x = 0, \end{cases} \tag{7}$$

$$\mathrm{sig_n^{\alpha}}(x) \triangleq \|x\|^{\alpha}\mathrm{sign_n}(x). \tag{8}$$

Remark 2. The norm-normalized sign function in (8) normalizes an input vector with its norm and works as a direction vector. Both Eq. (7) and the classical sign function in (5) share the property of directionality; therefore it is called a norm-normalized sign function. Similar functions include the scaled unit vector [30], and the vector-valued function [31].

3 Fixed-time-synchronized control for input-dimension-dominant systems

The matrix A_{12} of the MIMO system (3), in the input-dimension-dominant case, has the dimension of $(n-m)\times m$ where $m \geqslant \frac{n}{2}$. The following assumption is made on A_{21} for proper controller design.

Assumption 2. The right inverse of matrix $A_{12} \in \mathbb{R}^{(n-m)\times m}$ exists.

Before dealing with MIMO systems, we present the following lemma.

Lemma 4. Consider the following sliding mode surface s:

$$s = \dot{x} + p\ \mathrm{sig}_{\mathrm{n}}^{\alpha}(x) + g\ \mathrm{sig}_{\mathrm{n}}^{\beta}(x), \tag{9}$$

where p, g, α, β are positive parameters with $0 < \alpha < 1$ and $\beta > 1$. The system state x is ratio persistent and converges time-synchronously within a fixed time interval if $s = 0$, and the synchronized settling time can be formulated as

$$T \leqslant 2^{\frac{1-\alpha}{2}}/(p(1-\alpha)) + 2^{\frac{1-\beta}{2}}/(g(\beta-1)). \tag{10}$$

Proof. When $s = 0$, Eq. (9) becomes

$$\dot{x} = -p\ \mathrm{sig}_{\mathrm{n}}^{\alpha}(x) - g\ \mathrm{sig}_{\mathrm{n}}^{\beta}(x), \tag{11}$$

which leads to

$$\frac{\dot{x}}{\|\dot{x}\|} = \frac{-p\ \mathrm{sig}_{\mathrm{n}}^{\alpha}(x) - g\ \mathrm{sig}_{\mathrm{n}}^{\beta}(x)}{\|p\ \mathrm{sig}_{\mathrm{n}}^{\alpha}(x) + g\ \mathrm{sig}_{\mathrm{n}}^{\beta}(x)\|} = -\frac{(p\|x\|^{\alpha} + g\|x\|^{\beta})\mathrm{sign}_{\mathrm{n}}(x)}{\|(p\|x\|^{\alpha} + g\|x\|^{\beta})\,\mathrm{sign}_{\mathrm{n}}(x)\|} = -\frac{\mathrm{sign}_{\mathrm{n}}(x)}{\|\mathrm{sign}_{\mathrm{n}}(x)\|} = -\frac{x}{\|x\|}; \tag{12}$$

thus x is ratio persistent as defined in Lemma 2.

Consider $V = \frac{1}{2}x^{\mathrm{T}}x$ with the derivative

$$\dot{V} = -px^{\mathrm{T}}\mathrm{sig}_{\mathrm{n}}^{\alpha}(x) - gx^{\mathrm{T}}\mathrm{sig}_{\mathrm{n}}^{\beta}(x) = -p\|x\|^{\alpha+1} - g\|x\|^{\beta+1} = -2^{\frac{1+\alpha}{2}}pV^{\frac{1+\alpha}{2}} - 2^{\frac{1+\beta}{2}}gV^{\frac{1+\beta}{2}}. \tag{13}$$

According to Lemma 1, the settling time has the formulation of (10).

With the above lemma, we can deal with the fixed-time-synchronized control of MIMO systems. The following assumption is made on the perturbation.

Assumption 3. The disturbances and their derivatives in system (3) satisfy the following equations:

$$\|d_1\| \leqslant \eta_1\,\|x\| + h_1,\ \ \|d_2\| \leqslant \eta_2\,\|u\| + h_2,\ \ \|\dot{d}_1\| \leqslant \kappa_1\,\|x\| + \vartheta_1,\ \ \|\dot{d}_2\| \leqslant \kappa_2\,\|u\| + \vartheta_2, \tag{14}$$

where η_1, η_2, κ_1, κ_2, and ϑ_1 are known positive constants, $0 < h_1 < 1$, h_2 and ϑ_2 are known positive functions.

Remark 3. Assumption 3 is commonly used in [14, 32], which makes the controller design easier for uncertain disturbed systems. In Assumption 3, d_2 meets the so-called matching condition [33]. It is called the matched disturbance because it appears in the control channel and can be compensated directly by the control input. Correspondingly, d_1 is called the unmatched disturbance and appears outside the control channel. It cannot be eliminated directly by the control input, therefore it is more challenging than the matched disturbance. In this study, we consider both kinds of disturbances.

The fixed-time-synchronized controller is designed using the back-stepping architecture, where x_2 is regarded as the control input of x_1 that forces every element of x_1 to converge simultaneously.

A terminal sliding mode surface is designed for x_1,

$$s_1 = \dot{x}_1 + p_1\mathrm{sig}_{\mathrm{n}}^{\alpha_1}(x_1) + g_1\mathrm{sig}_{\mathrm{n}}^{\beta_1}(x_1), \tag{15}$$

where $p_1, g_1, \alpha_1, \beta_1$ are positive parameters with $0 < \alpha_1 < 1$ and $\beta_1 > 1$.

The sliding mode surface has the same structure as in (9). According to Lemma 4, x_1 converges time-synchronously within

$$T_1 \leqslant 2^{\frac{1-\alpha_1}{2}}/(p_1(1-\alpha_1)) + 2^{\frac{1-\beta_1}{2}}(g_1(\beta_1-1)), \tag{16}$$

if s_1 remains zero.

In order to drive s_1 to zero, a virtual control input ϕ is designed as follows:

$$\phi = \phi_1 + \phi_2, \tag{17}$$
$$\phi_1 = -A_{12}^{\dagger}\left(A_{11}x_1 + p_1\mathrm{sig}_{\mathrm{n}}^{\alpha_1}(x_1) + g_1\mathrm{sig}_{\mathrm{n}}^{\beta_1}(x_1)\right), \tag{18}$$
$$\dot{\phi}_2 = -A_{12}^{\dagger}\left(\Upsilon_1\mathrm{sign}_{\mathrm{n}}(s_1) + p_2\mathrm{sig}_{\mathrm{n}}^{\alpha_2}(s_1) + g_2\mathrm{sig}_{\mathrm{n}}^{\beta_2}(s_1)\right), \tag{19}$$
$$\Upsilon_1 = \kappa_1\|x\| + \vartheta_1, \tag{20}$$

where $p_2, g_2, \alpha_2, \beta_2$ are positive parameters with $0 < \alpha_2 < 1$ and $\beta_2 > 1$. $A_{12}^{\dagger}$ is the right inverse of A_{12}.

Let the deviation between ϕ and x_2 be z, namely $z = x_2 - \phi$. In what follows, we will show that if $\dot{z} = z = 0$, s_1 converges in a fixed time interval.

In (17), the formulation of ϕ consists of two parts. The first item ϕ_1 is designed to shape $\dot{x}_1$ and to force s_1 to its equilibrium. The derivative of the second item ϕ_2 is designed to eliminate the varying disturbances and to shape the changing rate of an s_1-based Lyapunov function.

Lemma 5. When $z = \dot{z} = 0$, the system (3) converges to the sliding surface $s_1 = 0$.

Proof. When $z = \dot{z} = 0$, the system state x_2 has the same value as the virtual control signal ϕ, namely $x_2 = \phi$, which leads to $\dot{x}_1 = A_{11}x_1 + A_{12}\phi + d_1$. Substituting $\dot{x}_1$ into the sliding mode surface s_1 in (15) yields

$$s_1 = A_{11}x_1 + A_{12}\phi + d_1 + p_1\mathrm{sig}_{\mathrm{n}}^{\alpha_1}(x_1) + g_1\mathrm{sig}_{\mathrm{n}}^{\beta_1}(x_1). \tag{21}$$

Substituting (17) into the above equation yields $s_1 = A_{12}\phi_2 + d_1$.

Considering a Lyapunov candidate $V_1 = \frac{1}{2}s_1^{\mathrm{T}}s_1$, it has the following derivative:

$$\dot{V}_1 = s_1^{\mathrm{T}}(A_{12}\dot{\phi}_2 + \dot{d}_1) = s_1^{\mathrm{T}}\dot{d}_1 - s_1^{\mathrm{T}}\left(\Upsilon_1\mathrm{sign}_{\mathrm{n}}(s_1) + p_2\mathrm{sig}_{\mathrm{n}}^{\alpha_2}(s_1) + g_2\mathrm{sig}_{\mathrm{n}}^{\beta_2}(s_1)\right).$$

According to the definition of $\mathrm{sig}_{\mathrm{n}}^{\alpha}(\cdot)$ and our assumption of the changing rate of the disturbance d_1,

$$\begin{aligned}\dot{V}_1 \leqslant & -\Upsilon_1(x)\|s_1\| - p_2\|s_1\|^{\alpha_2+1} - g_2\|s_1\|^{\beta_2+1} + \|s_1\|(\kappa_1\|x\| + \vartheta_1)\\ \leqslant & -p_2\|s_1\|^{\alpha_2+1} - g_2\|s_1\|^{\beta_2+1} = -2^{\frac{1+\alpha_2}{2}}p_2V_1^{\frac{1+\alpha_2}{2}} - 2^{\frac{1+\beta_2}{2}}g_2V_1^{\frac{1+\beta_2}{2}}.\end{aligned} \tag{22}$$

According to Lemma 1, the output signal x_1 converges to the sliding mode surface $s_1 = 0$ within the following fixed settling time:

$$T_2 \leqslant 2^{\frac{1-\alpha_2}{2}}/(p_2(1-\alpha_2)) + 2^{\frac{1-\beta_2}{2}}/(g_2(\beta_2-1)), \tag{23}$$

which completes the proof.

Next, the deviation between x_2 and its desired value ϕ will be controlled to zero. The time-synchronized terminal sliding mode surface s_2 is defined on z,

$$s_2 = \dot{z} + p_3\mathrm{sig}_{\mathrm{n}}^{\alpha_3}(z) + g_3\mathrm{sig}_{\mathrm{n}}^{\beta_3}(z), \tag{24}$$

where $p_3, g_3, \alpha_3, \beta_3$ are positive parameters with $0 < \alpha_3 < 1$ and $\beta_3 > 1$.

The sliding mode surface has exactly the same structure as in (9) and (15). According to Lemma 4, if s_2 remains zero, z converges time-synchronously within

$$T_3 \leqslant 2^{\frac{1-\alpha_3}{2}}/(p_3(1-\alpha_3)) + 2^{\frac{1-\beta_3}{2}}(g_3(\beta_3-1)). \tag{25}$$

In order to drive the sliding mode surface s_2 to zero and make z converge time-synchronously, the control input u is designed based on s_2,

$$u = u_1 + u_2, \tag{26}$$

$$\begin{aligned} u_1 =& -\left(A_{21}x_1 + A_{22}x_2 + p_3\mathrm{sig}_{\mathrm{n}}^{\alpha_3}(z) + g_3\mathrm{sig}_{\mathrm{n}}^{\beta_3}(z)\right) - A_{12}^{\dagger}\left(\Upsilon_1\mathrm{sign}_{\mathrm{n}}(s_1) + p_2\mathrm{sig}_{\mathrm{n}}^{\alpha_2}(s_1) + g_2\mathrm{sig}_{\mathrm{n}}^{\beta_2}(s_1)\right) \\ & - A_{12}^{\dagger}\left(A_{11} + \varphi(x_1)\right)\left(A_{11}x_1 + A_{12}x_2\right), \end{aligned} \tag{27}$$

$$\dot{u}_2 = -\Upsilon_2\mathrm{sign}_{\mathrm{n}}(s_2) - \left(p_4\mathrm{sig}_{\mathrm{n}}^{\alpha_4}(s_2) + g_4\mathrm{sig}_{\mathrm{n}}^{\beta_4}(s_2)\right), \tag{28}$$

$$\Upsilon_2 = \kappa_2\|u_1\| + \vartheta_2 + \|A_{12}^{\dagger}(A_{11} + \varphi(x_1))\|(\kappa_1\|x\| + \vartheta_1) + \|A_{12}^{\dagger}\dot{\varphi}(x_1)\|\,\|\eta_1\|x\| + h_1\| + \kappa_2\left\|\int_0^t \dot{u}_2\mathrm{d}t\right\|, \tag{29}$$

where $p_4, g_4, \alpha_4, \beta_4$ are positive parameters with $0 < \alpha_4 < 1$ and $\beta_4 > 1$, and $\varphi(x_1)$ is a function defined as

$$\varphi(x_1) = p_1(\alpha_1 - 1)\|x_1\|^{\alpha_1 - 3}x_1x_1^{\mathrm{T}} + p_1\|x_1\|^{\alpha_1 - 1}I_{n-m} + g_1(\beta_1 - 1)\|x_1\|^{\beta_1 - 3}x_1x_1^{\mathrm{T}} + g_1\|x_1\|^{\beta_1 - 1}I_{n-m}.$$

The controller (26) is quasi-continuous and should be understood in the Filippov sense [34].

Theorem 1. Considering the input-dimension-dominant case of the MIMO system (3), under Assumptions 1–3, using the control input (26) and the virtual control signal (17), the tracking error z and the output $y = x_1$ will reach the sliding mode surfaces $s_2 = 0$ and $s_1 = 0$ in fixed-time, then move along these terminal sliding surfaces, and finally converge to their equilibrium time-synchronously within a fixed time interval.

Proof. Firstly, let us show that the tracking error z reaches the sliding mode surface $s_2 = 0$ in fixed time. Substituting $z = x_2 - \phi$ into (24), the sliding mode surface s_2 becomes

$$\begin{aligned} s_2 =& \dot{x}_2 - \dot{\phi} + p_3\mathrm{sig}_{\mathrm{n}}^{\alpha_3}(z) + g_3\mathrm{sig}_{\mathrm{n}}^{\beta_3}(z) \\ =& A_{21}x_1 + A_{22}x_2 + u + d_2 + p_3\mathrm{sig}_{\mathrm{n}}^{\alpha_3}(z) + g_3\mathrm{sig}_{\mathrm{n}}^{\beta_3}(z) + A_{12}^{\dagger}\left(\Upsilon_1\mathrm{sign}_{\mathrm{n}}(s_1) + p_2\mathrm{sig}_{\mathrm{n}}^{\alpha_2}(s_1) + g_2\mathrm{sig}_{\mathrm{n}}^{\beta_2}(s_1)\right) \\ & + \frac{\mathrm{d}}{\mathrm{d}t}\left(A_{12}^{\dagger}\left(A_{11}x_1 + p_1\mathrm{sig}_{\mathrm{n}}^{\alpha_1}(x_1) + g_1\mathrm{sig}_{\mathrm{n}}^{\beta_1}(x_1)\right)\right). \end{aligned} \tag{30}$$

In the above equation, the time derivative of $\mathrm{sig}_{\mathrm{n}}^{\alpha}(x)$ is used. From $\|x\| = (x^{\mathrm{T}}x)^{\frac{1}{2}}$,

$$\frac{\mathrm{d}}{\mathrm{d}t}\mathrm{sig}_{\mathrm{n}}^{\alpha}(x) = \frac{\mathrm{d}}{\mathrm{d}t}\left(\|x\|^{\alpha}\frac{x}{\|x\|}\right) = \frac{\mathrm{d}}{\mathrm{d}t}\|x\|^{\alpha - 1}x = \left(\|x\|^{\alpha - 1} + (\alpha - 1)\|x\|^{\alpha - 3}xx^{\mathrm{T}}\right)\dot{x}. \tag{31}$$

Then, Eq. (30) can be written as

$$\begin{aligned} s_2 =& A_{21}x_1 + A_{22}x_2 + u + d_2 + p_3\mathrm{sig}_{\mathrm{n}}^{\alpha_3}(z) + g_3\mathrm{sig}_{\mathrm{n}}^{\beta_3}(z) + A_{12}^{\dagger}\left(\Upsilon_1\mathrm{sign}_{\mathrm{n}}(s_1) + p_2\mathrm{sig}_{\mathrm{n}}^{\alpha_2}(s_1) + g_2\mathrm{sig}_{\mathrm{n}}^{\beta_2}(s_1)\right) \\ & + A_{12}^{\dagger}\left(A_{11} + \varphi(x_1)\right)\left(A_{11}x_1 + A_{12}x_2\right) + A_{12}^{\dagger}\left(A_{11} + \varphi(x_1)\right)d_1. \end{aligned} \tag{32}$$

Under the control input (26),

$$s_2 = u_2 + d_2 + A_{12}^{\dagger}\left(A_{11} + \varphi(x_1)\right)d_1. \tag{33}$$

Correspondingly, the derivative of s_2 is

$$\dot{s}_2 = \dot{u}_2 + \dot{d}_2 + A_{12}^{\dagger}\left(A_{11} + \varphi(x_1)\right)\dot{d}_1 + A_{12}^{\dagger}\dot{\varphi}(x_1)d_1. \tag{34}$$

Considering a Lyapunov candidate $V_2 = \frac{1}{2}s_2^{\mathrm{T}}s_2$, it has the following derivative:

$$\dot{V}_2 = s_2^{\mathrm{T}}\left(\dot{u}_2 + \dot{d}_2 + A_{12}^{\dagger}(A_{11} + \varphi(x_1))\dot{d}_1 + A_{12}^{\dagger}\dot{\varphi}(x_1)d_1\right). \tag{35}$$

According to Assumption 3,

$$\begin{aligned} \dot{V}_2 \leqslant & \|s_2\|\left(\kappa_2\|u\| + \vartheta_2\right) + \|s_2\|\|A_{12}^{\dagger}\dot{\varphi}(x_1)\|\left(\eta_1\|x\| + h_1\right) \\ & + s_2^{\mathrm{T}}\dot{u}_2 + \|s_2\|\|A_{12}^{\dagger}\left(A_{11} + \varphi(x_1)\right)\|\left(\kappa_1\|x\| + \vartheta_1\right). \end{aligned} \tag{36}$$

Substituting (26) into the above equation and recalling the formulation of ${\mathrm{sign}_{\mathrm{n}}}^{\alpha}(x)$, we have

$$\begin{aligned} \dot{V}_2 \leqslant & -s_2^{\mathrm{T}}\left(\Upsilon_2\mathrm{sign}_{\mathrm{n}}(s_2) + p_4\mathrm{sig}_{\mathrm{n}}^{\alpha_4}(s_2) + g_4\mathrm{sig}_{\mathrm{n}}^{\beta_4}(s_2)\right) + \vartheta_2\|s_2\| + \|s_2\|\|A_{12}^{\dagger}\left(A_{11} + \varphi(x_1)\right)\|\left(\kappa_1\|x\| + \vartheta_1\right) \\ & + \kappa_2\|s_2\|\left(\|u_1\| + \|u_2\|\right) + \|s_2\|\|A_{12}^{\dagger}\dot{\varphi}(x_1)\|\left(\eta_1\|x\| + h_1\right) \end{aligned}$$

$$
\begin{aligned}
&\leqslant -p_4\mathrm{sig}_{\mathrm{n}}^{\alpha_4}(s_2) - g_4\mathrm{sig}_{\mathrm{n}}^{\beta_4}(s_2) = -p_4\|s_2\|^{\alpha_4+1} - g_4\|s_2\|^{\beta_4+1} \\
&\leqslant -2^{\frac{\alpha_4+1}{2}}p_4V_2^{\frac{\alpha_4+1}{2}} - 2^{\frac{\alpha_4+1}{2}}g_4V_2^{\frac{\beta_4+1}{2}},
\end{aligned} \tag{37}
$$

which is fixed-time stable according to Lemma 1, and the settling time for the convergence of s_2 is

$$
T_4 \leqslant 2^{\frac{1-\alpha_4}{2}}/(p_4(1-\alpha_4)) + 2^{\frac{1-\beta_4}{2}}/(g_4(\beta_4-1)). \tag{38}
$$

After s_2 converges to zero within T_4, the tracking error z moves along the sliding mode surface $s_2 = 0$ and converges to zero time-synchronously within T_3. Then, $z = \dot{z} = 0$, the sliding mode surface s_1 converges to zero within a fixed time interval T_2 according to Lemma 5. As $s_1 = 0$, the system output s_1 converges to zero time-synchronously within T_1. The bound of the setting time for the whole process can be formulated as

$$
T_{\mathrm{idd}} \leqslant T_1 + T_2 + T_3 + T_4, \tag{39}
$$

where T_1, T_2, T_3 and T_4 are specified in (16), (23), (25), and (38), respectively.

Remark 4. The bound of the setting time for the whole process is estimated as T_{idd}, which consists of four parts as analyzed above. Although still larger than the true convergence time, it is less conservative than the estimation in conventional methods [10, 32]. This is because on the terminal sliding mode surfaces $s_1 = 0$ and $s_2 = 0$, the derivatives of the Lyapunov functions V_1 and V_2 are calculated as accurate values and not relaxed. Correspondingly, the settling time calculated based on $\dot{V}_1$ and $\dot{V}_2$ is not very over-estimated.

The singularity problem widely exists in sliding-mode-based controllers. Note that φ in the controller (26) may result in the singularity problem at $\|x_1\| \to 0$ since $\alpha_1 < 1$.

In what follows, the controller (26) is re-designed to be singularity-free.

The terminal sliding-mode surface with respect to x_1 is constructed in the following form:

$$
s_1 = \dot{x}_1 + s_s, \tag{40}
$$

where s_s is formulated as

$$
s_s = \begin{cases} p_1\mathrm{sig}_{\mathrm{n}}^{\alpha_1}(x_1) + g_1\mathrm{sig}_{\mathrm{n}}^{\beta_1}(x_1), & \text{if } s^* = 0 \text{ or } s^* \neq 0,\ \|x_1\| > \varepsilon, \\ l_1x_1 + l_2\mathrm{sig}_{\mathrm{n}}^{4}(x_1), & \text{if } s^* \neq 0,\ \|x_1\| \leqslant \varepsilon, \end{cases} \tag{41}
$$

where ε is a small constant, s^* is the triggering variable $s^* = \dot{x}_1 + p_1\mathrm{sig}_{\mathrm{n}}^{\alpha_1}(x_1) + g_1\mathrm{sig}_{\mathrm{n}}^{\beta_1}(x_1)$ with $p_1 > 0, g_1 > 0, 0.5 < \alpha_1 < 1, \beta_1 > 1$, and l_1 and l_2 are constants that take the following forms:

$$
l_1 = \alpha_1\left(\frac{4}{3} - \frac{p_1}{3}\right)\|\varepsilon\|^{p_1-1} + \beta_1\left(\frac{4}{3} - \frac{g_1}{3}\right)\|\varepsilon\|^{g_1-1},\ l_2 = \alpha_1\left(\frac{p_1}{3} - \frac{1}{3}\right)\|\varepsilon\|^{p_1-4} + \beta_1\left(\frac{g_1}{3} - \frac{1}{3}\right)\|\varepsilon\|^{g_1-4}. \tag{42}
$$

Note that s_s is continuous at $\|x_1\| = \varepsilon$.

Lemma 6. Using the sliding-mode surfaces (24) and (40), the virtual control signal (17), and the controller (26) with a modified $\varphi(x_1)$ constructed as

$$
\varphi(x_1) = \begin{cases} \left(l_1 + 3\|x_1\|x_1x_1^{\mathrm{T}} + l_2\|x_1\|^3\right)(A_{11}x_1 + A_{12}x_2), & \text{if } s^* = 0 \text{ or } s^* \neq 0,\ \|x_1\| > \varepsilon, \\ p_1^2\alpha_1\mathrm{sig}_{\mathrm{n}}^{2\alpha_1-1}(x_1) + g_1^2\beta_1\mathrm{sig}_{\mathrm{n}}^{2\beta_1-1}(x_1) + p_1g_1(\alpha_1+\beta_1)\mathrm{sig}_{\mathrm{n}}^{\alpha_1+\beta_1-1}(x_1), & \text{if } s^* \neq 0,\ \|x_1\| \leqslant \varepsilon, \end{cases}
$$

the singularity problem can be avoided.

Proof. The analysis is conducted in three cases.

(1) $\|x_1\| > \varepsilon$, with which the singularity does not exist and the stability analysis in Theorem 1 works.

(2) $\|x_1\| \leqslant \varepsilon$ and $s^* \neq 0$, with which the $\varphi(x_1)$ in u_1 becomes $(l_1 + 3\|x_1\|x_1x_1^{\mathrm{T}} + l_2\|x_1\|^3)(A_{11}x_1 + A_{12}x_2)$. Also, no singularity exists apparently.

Since the sliding-mode surface s_1 is designed differently, the time-synchronized property and stability are discussed here. When $s_1 = 0$,

$$
\frac{\dot{x}_1}{\|\dot{x}_1\|} = -\frac{l_1x_1 + l_2\mathrm{sig}_{\mathrm{n}}^{4}(x_1)}{\|l_1x_1 + l_2\mathrm{sig}_{\mathrm{n}}^{4}(x_1)\|} = -\frac{(l_1\|x_1\| + l_2\|x_1\|^4)\mathrm{sign}_{\mathrm{n}}(x_1)}{\|(l_1\|x_1\| + l_2\|x_1\|^4)\,\mathrm{sign}_{\mathrm{n}}(x_1)\|} = \pm\frac{x_1}{\|x_1\|}, \tag{43}
$$

which indicates that x_1 is still ratio persistent and the time-synchronized property remains. Consider the Lypuanov function $V = x_1^{\mathrm{T}} x_1$, whose time derivative is

$$\dot{V} = x_1^{\mathrm{T}} \dot{x}_1 = -2x_1^{\mathrm{T}} \left(l_1 x_1 + l_2 \mathrm{sig}_{\mathrm{n}}^4(x_1) \right) \leqslant 0; \tag{44}$$

thus x_1 converges time-synchronously when $s_1 = 0$ in this case.

As the formulations of ϕ and s_2 are not modified, it is easy to achieve that the system (3) converges to $s_1 = 0$ when $z = \dot{z} = 0$, namely $x_2 = \phi$, and z converges time-synchronously when $s_2 = 0$.

Next, we will show that the control input u drives s_2 to the equilibrium. Substituting $z = x_2 - \phi$ into (24), the sliding mode surface s_2 becomes

$$\begin{aligned} s_2 =& \dot{x}_2 - \dot{\phi} + p_3 \mathrm{sig}_{\mathrm{n}}^{\alpha_3}(z) + g_3 \mathrm{sig}_{\mathrm{n}}^{\beta_3}(z) \\ =& A_{21} x_1 + A_{22} x_2 + u + d_2 + A_{12}^{\dagger} \left(\Upsilon_1 \mathrm{sign}_{\mathrm{n}}(s_1) + p_2 \mathrm{sig}_{\mathrm{n}}^{\alpha_2}(s_1) + g_2 \mathrm{sig}_{\mathrm{n}}^{\beta_2}(s_1) \right) \\ &+ p_3 \mathrm{sig}_{\mathrm{n}}^{\alpha_3}(z) + g_3 \mathrm{sig}_{\mathrm{n}}^{\beta_3}(z) + A_{12}^{\dagger} \left(A_{11} + l_1 + 3\|x_1\| x_1 x_1^{\mathrm{T}} + l_2 \|x_1\|^3 \right) (A_{11} x_1 + A_{12} x_2). \end{aligned} \tag{45}$$

Under the control input (26), $s_2 = u_2 + d_2 + A_{12}^{\dagger} \left(A_{11} + \varphi(x_1) \right) d_1$, which is the same as (33). Following the analysis of Theorem 1, the convergence of z and the system (3) can be proved.

Therefore, the system is time-synchronized stable without singularity in this case.

(3) $\|x_1\| \leqslant \varepsilon$ and $s^* = 0$. In this case, s_1, ϕ, and s_2 are still the formulations of (15), (17), and (24); thus the system is fixed-time-synchronized stable if the control input u can drive z to fixed-time convergence.

Substituting $z = x_2 - \phi$ into (24), the sliding mode surface s_2 becomes

$$\begin{aligned} s_2 =& \dot{x}_2 - \dot{\phi} + p_3 \mathrm{sig}_{\mathrm{n}}^{\alpha_3}(z) + g_3 \mathrm{sig}_{\mathrm{n}}^{\beta_3}(z) \\ =& A_{21} x_1 + A_{22} x_2 + u + d_2 + A_{12}^{\dagger} \left(\Upsilon_1 \mathrm{sign}_{\mathrm{n}}(s_1) + p_2 \mathrm{sig}_{\mathrm{n}}^{\alpha_2}(s_1) + g_2 \mathrm{sig}_{\mathrm{n}}^{\beta_2}(s_1) \right) \\ &+ p_3 \mathrm{sig}_{\mathrm{n}}^{\alpha_3}(z) + g_3 \mathrm{sig}_{\mathrm{n}}^{\beta_3}(z) + \frac{\mathrm{d}}{\mathrm{d}t} \left(A_{12}^{\dagger} \left(A_{11} x_1 + p_1 \mathrm{sig}_{\mathrm{n}}^{\alpha_1}(x_1) + g_1 \mathrm{sig}_{\mathrm{n}}^{\beta_1}(x_1) \right) \right). \end{aligned} \tag{46}$$

Recall that in this case $s^* = \dot{x}_1 + p_1 \mathrm{sig}_{\mathrm{n}}^{\alpha_1}(x_1) + g_1 \mathrm{sig}_{\mathrm{n}}^{\beta_1}(x_1) = 0$ and it follows that

$$\begin{aligned} &\frac{\mathrm{d}}{\mathrm{d}t} \left(A_{12}^{\dagger} \left(p_1 \mathrm{sig}_{\mathrm{n}}^{\alpha_1}(x_1) + g_1 \mathrm{sig}_{\mathrm{n}}^{\beta_1}(x_1) \right) \right) \\ &= -A_{12}^{\dagger} \left(p_1(\alpha_1 - 1) \|x_1\|^{\alpha_1 - 3} x_1 x_1^{\mathrm{T}} + p_1 \|x_1\|^{\alpha_1 - 1} I_{n-m} \right) \left(p_1 \mathrm{sig}_{\mathrm{n}}^{\alpha_1}(x_1) + g_1 \mathrm{sig}_{\mathrm{n}}^{\beta_1}(x_1) \right) \\ &\quad - A_{12}^{\dagger} \left(g_1(\beta_1 - 1) \|x_1\|^{\beta_1 - 3} x_1 x_1^{\mathrm{T}} + g_1 \|x_1\|^{\beta_1 - 1} I_{n-m} \right) \left(p_1 \mathrm{sig}_{\mathrm{n}}^{\alpha_1}(x_1) + g_1 \mathrm{sig}_{\mathrm{n}}^{\beta_1}(x_1) \right). \end{aligned}$$

From $x_1 x_1^{\mathrm{T}} \mathrm{sig}_{\mathrm{n}}^{\alpha_1}(x_1) = \mathrm{sig}_{\mathrm{n}}^{\alpha_1 + 2}(x_1)$,

$$\begin{aligned} &\frac{\mathrm{d}}{\mathrm{d}t} \left(A_{12}^{\dagger} \left(p_1 \mathrm{sig}_{\mathrm{n}}^{\alpha_1}(x_1) + g_1 \mathrm{sig}_{\mathrm{n}}^{\beta_1}(x_1) \right) \right) \\ &\quad = p_1^2 \alpha_1 \mathrm{sig}_{\mathrm{n}}^{2\alpha_1 - 1}(x_1) + g_1^2 \mathrm{sig}_{\mathrm{n}}^{2\beta_1 - 1}(x_1) + p_1 g_1 (\alpha_1 + \beta_1) \mathrm{sig}_{\mathrm{n}}^{\alpha_1 + \beta_1 - 1}(x_1). \end{aligned} \tag{47}$$

Invoking (46), (26), and (47), we have $s_2 = u_2 + d_2 + A_{12}^{\dagger} A_{11} d_1$, which is similar to (33). Following the analysis of Theorem 1, the convergence of z and the system (3) can be proved.

Moreover, the $\varepsilon(x_1)$ in this case is nonsingular at $0.5 < \alpha_1 < 1$ and $\beta_1 > 1$. Therefore, the system is singularity-free.

4 Semi-fixed-time-synchronized control for state-dimension-dominant MIMO systems

In this section, we consider the state-dimension-dominant case where the input dimension is smaller than the output dimension, namely $m < \frac{n}{2}$ for system (3). In this case, the system matrix A_{12} in (3) does not have a right inverse, which increases the difficulty of the controller design. Moreover, when the system state x_2 is treated as the control input of x_1, it is not powerful enough to shape an arbitrary output trajectory because the dimension of x_2 is smaller than the dimension of x_1. Due to the limited capability of the control input, the state-dimension-dominant system cannot achieve the ideal fixed-time-synchronized convergence. Instead, we can expect parts of the output components to converge simultaneously in fixed time, which is said to be semi-fixed-time-synchronized stable.

In what follows, the system (3) is considered in the case of $m < \frac{n}{2}$. We aim to design a controller that brings l ($l \leqslant m$) output dimensions to the semi-time-synchronized convergence, where l is the controllability index of the system $\dot{x}_1 = A_{11}x_1 + A_{12}x_2 + d_1(t,x)$.

Despite Assumption 3 that is made on the disturbance d_2, we make another assumption on d_1 for the convenience of the subsequent system transformation.

Assumption 4. The disturbance d_1 can be written as $d_1 = A_{12}\omega(t,x)$, where $\omega(t,x)$ is considered as a transformed formulation of the unmatched disturbance in the following analysis. Moreover, $\omega(t,x)$ and its first-order time derivative are both bounded,

$$\|\omega(t,x)\| \leqslant \eta_3 \|x\| + h_3,\ \ \|\dot{\omega}(t,x)\| \leqslant \kappa_3 \|x\| + \vartheta_3, \tag{48}$$

where η_3, h_3, κ_3 and ϑ_3 are known positive parameters.

Hereinafter, ω is used instead of $\omega(t,x)$ for short.

Inspired by [35], a state transformation is taken for the first part of system (3),

$$x_1 = \Gamma_1^{-1}\Gamma_2 v,\ \ v = \Gamma_2^{-1}\Gamma_1 x_1. \tag{49}$$

where v is the transformed system state, Γ_1 and Γ_2 are system transformation matrices (the detailed formulations are omitted, please refer to [36] for Γ_1 and [29] for Γ_2).

$$\begin{bmatrix} \dot{x}'_r \\ \dot{x}'_{r-1} \\ \vdots \\ \dot{x}'_3 \\ \dot{x}'_2 \\ \dot{x}'_1 \end{bmatrix} = \begin{bmatrix} A'_{r,r} & B'_{r,r-1} & \cdots & 0 & 0 & 0 \\ A'_{r-1,r} & A'_{r-1,r-1} & \cdots & 0 & 0 & 0 \\ \vdots & \vdots & \ddots & \vdots & \vdots & \vdots \\ A'_{3,r} & A'_{3,r-1} & \cdots & A'_{3,3} & B'_{3,2} & 0 \\ A'_{2,r} & A'_{2,r-1} & \cdots & A'_{2,3} & A'_{2,2} & B'_{2,1} \\ A'_{1,r} & A'_{1,r-1} & \cdots & A'_{1,3} & A'_{1,2} & A'_{1,1} \end{bmatrix} \begin{bmatrix} x'_r \\ x'_{r-1} \\ \vdots \\ x'_3 \\ x'_2 \\ x'_1 \end{bmatrix} + \begin{bmatrix} 0 \\ 0 \\ \vdots \\ 0 \\ 0 \\ B_{1,0}\left(x_2+\omega\right) \end{bmatrix},$$

$$\begin{bmatrix} \dot{v}_r \\ \dot{v}_{r-1} \\ \vdots \\ \dot{v}_3 \\ \dot{v}_2 \\ \dot{v}_1 \end{bmatrix} = \begin{bmatrix} \bar{A}_r & B'_{r,r-1} & \cdots & 0 & 0 & 0 \\ 0 & \bar{A}_{r-1} & \cdots & 0 & 0 & 0 \\ \vdots & \vdots & \ddots & \vdots & \vdots & \vdots \\ 0 & 0 & \cdots & \bar{A}_3 & B'_{3,2} & 0 \\ 0 & 0 & \cdots & 0 & \bar{A}_2 & B'_{2,1} \\ A''_{1,r} & A''_{1,r-1} & \cdots & A''_{1,3} & A''_{1,2} & A''{}_{1,1} \end{bmatrix} \begin{bmatrix} v_r \\ v_{r-1} \\ \vdots \\ v_3 \\ v_2 \\ v_1 \end{bmatrix} + \begin{bmatrix} 0 \\ 0 \\ \vdots \\ 0 \\ B_{1,0}\left(x_2+\omega\right) \end{bmatrix}. \tag{50}$$

The transformation is conducted in two steps, namely $x' = \Gamma_1 x_1$ and $v = \Gamma_2^{-1}x'$, which are illustrated in (50). With the first transformation, the system can be rewritten as the block controllable form in (50), where an "invertible part" can be extracted from A_{12}. With the second transformation, the system state $v_i, i = 2, \ldots, r$ is further decoupled.

In (50), the column rank of $B'_{1,0}$ is the same as x'_1 and v_1; thus it is possible to calculate the right inverse of $B'_{1,0}$. Furthermore, it indicates the output components of v_1 can be controlled ideally and driven to their equilibrium simultaneously. Since $\operatorname{rank}(B'_{i,i-1}) = \dim\left(x'_i\right),\ i = 2, \ldots, r$, the right inverse of $B'_{i,i-1}$ exists although not used in the following derivations.

Based on the above transformation, system (3) can be re-written as

$$\begin{aligned} \dot{v}_i =& \bar{A}_i v_i + B'_{i,i-1}v_{i-1}, \quad i = 2, \ldots, r, \\ \dot{v}_1 =& \sum_{i=1}^{r} A''_{1,i}v_i + B_{1,0}\left(x_2+\omega\right), \\ \dot{x}_2 =& A_{21}x_1 + A_{22}x_2 + u + d_2(t,x,u), \end{aligned} \tag{51}$$

where $\bar{A}_i$ is defined as $\bar{A}_i = -\lambda_i I_{\pi_i}$, λ_i is a positive parameter with $0 < \lambda_r < \cdots < \lambda_2$, and π_i denotes the dimension of v_i.

In system (51), v is the transformed formulation of state x_1 and the transformation is specified in (49). The system output is $y = v$, which cannot be driven to the origin at the same time due to the limited control capability. Instead, the control objective is the semi-time-synchronized stability, where v_1 is required to converge simultaneously.

Remark 5. The formulation of (51) shows why semi-time-synchronized convergence instead of time-synchronized convergence is accomplished in this section. With a properly designed controller, the elements of v_1 converge at the same time, and $v_2, \ldots, v_r$ will reach the origin one after another. Therefore only l output dimensions achieve time-synchronized convergence.

Similar to the input-dimension-dominant case, the system state x_2 is used as the control input for v_1. To achieve the fixed-time-synchronized convergence of v_1, a terminal sliding mode surface s_1 is defined,

$$s_1 = \dot{v}_1 + p_1 \mathrm{sig}_{\mathrm{n}}^{\alpha_1}(v_1) + g_1 \mathrm{sig}_{\mathrm{n}}^{\beta_1}(v_1), \tag{52}$$

where $p_1, g_1, \alpha_1, \beta_1$ are positive parameters with $0 < \alpha_1 < 1$ and $\beta_1 > 1$. According to Lemma 4, if $s_1 = 0$, the output signal v_1 converges time-synchronously within $T_1 \leqslant 2^{\frac{1-\alpha_1}{2}}/(p_1(1-\alpha_1)) + 2^{\frac{1-\beta_1}{2}}(g_1(\beta_1 - 1))$.

In order to force s_1 to the origin, a virtual control input ϕ is defined as follows:

$$\phi = \phi_1 + \phi_2, \tag{53}$$

$$\phi_1 = -B_{1,0}^{\dagger}\left(\sum_{i=1}^{r} A''_{1,i} v_i + p_1 \mathrm{sig}_{\mathrm{n}}^{\alpha_1}(v_1) + g_1 \mathrm{sig}_{\mathrm{n}}^{\beta_1}(v_1)\right), \tag{54}$$

$$\dot{\phi}_2 = -B_{1,0}^{\dagger}\left(\Upsilon_3 \mathrm{sign}_{\mathrm{n}}(s_1) + p_2 \mathrm{sig}_{\mathrm{n}}^{\alpha_2}(s_1) + g_2 \mathrm{sig}_{\mathrm{n}}^{\beta_2}(s_1)\right), \tag{55}$$

$$\Upsilon_3 = \|B_{1,0}\|(\kappa_3 \|x\| + \vartheta_3), \tag{56}$$

where $p_2, g_2, \alpha_2, \beta_2$ are positive parameters with $0 < \alpha_2 < 1$ and $\beta_2 > 1$. $B_{1,0}^{\dagger}$ is the right inverse of $B_{1,0}$.

Let the deviation between ϕ and x_2 be z, namely $z = x_2 - \phi$. In what follows, we will show that if $\dot{z} = z = 0$, s_1 converges in a fixed time.

In (17), the formulation of ϕ consists of two parts. The first item ϕ_1 is designed to shape $\dot{x}_1$ and to force s_1 to its equilibrium. The derivative of the second item ϕ_2 is designed to eliminate the varying disturbances and to shape the changing rate of an s_1-based Lyapunov function.

Lemma 7. When $z = \dot{z} = 0$, the output v_1 of the state-dimension-dominant MIMO system (51) converges to the sliding surface $s_1 = 0$.

Proof. When $z = \dot{z} = 0$, $x_2 = \phi$, which leads to

$$\dot{v}_1 = \sum_{i=1}^{r} A''_{1,i} v_i + B_{1,0}(\phi + \omega). \tag{57}$$

Combine the above equation with the formulation of the sliding mode surface s_1 in (52),

$$s_1 = \sum_{i=1}^{r} A''_{1,i} v_i + B_{1,0}(\phi + \omega) + p_1 \mathrm{sig}_{\mathrm{n}}^{\alpha_1}(x_1) + g_1 \mathrm{sig}_{\mathrm{n}}^{\beta_1}(x_1). \tag{58}$$

Substituting (53) into the above equation yields $s_1 = B_{1,0}(\phi_2 + \omega)$. Considering a Lyapunov candidate $V_1 = \frac{1}{2} s_1^{\mathrm{T}} s_1$, it has the following derivative:

$$\dot{V}_1 = s_1^{\mathrm{T}} B_{1,0}(\dot{\phi}_2 + \dot{\omega}) = -s_1^{\mathrm{T}}\left(\Upsilon_3 \mathrm{sign}_{\mathrm{n}}(s_1) + p_2 \mathrm{sig}_{\mathrm{n}}^{\alpha_2}(s_1) + g_2 \mathrm{sig}_{\mathrm{n}}^{\beta_2}(s_1) - B_{1,0}\dot{\omega}\right).$$

Recall the formulation of $\mathrm{sig}_{\mathrm{n}}^{\alpha}(\cdot)$ and the changing rate of the disturbance ω in Assumption 4,

$$\begin{aligned} \dot{V}_1 \leqslant & -\Upsilon_3 \|s_1\| - p_2 \|s_1\|^{\alpha_2+1} - g_2 \|s_1\|^{\beta_2+1} + \|s_1\| \|B_{1,0}\| (\kappa_3 \|x\| + \vartheta_3) \\ \leqslant & -p_2 \|s_1\|^{\alpha_2+1} - g_2 \|s_1\|^{\beta_2+1} = -2^{\frac{1+\alpha_2}{2}} p_2 V^{\frac{1+\alpha_2}{2}} - 2^{\frac{1+\beta_2}{2}} g_2 V^{\frac{1+\beta_2}{2}}. \end{aligned} \tag{59}$$

According to Lemma 1, the output signal v_1 converges to the sliding mode surface $s_1 = 0$ within the following fixed settling time:

$$T_2 \leqslant 2^{\frac{1-\alpha_2}{2}}/(p_2(1-\alpha_2)) + 2^{\frac{1-\beta_2}{2}}/(g_2(\beta_2 - 1)). \tag{60}$$

Next, the deviation between x_2 and its desired value ϕ will be controlled to zero. A time-synchronized terminal sliding mode surface is defined on z,

$$s_2 = \dot{z} + p_3\mathrm{sig}_\mathrm{n}^{\alpha_3}(z) + g_3\mathrm{sig}_\mathrm{n}^{\beta_3}(z), \tag{61}$$

where $p_3, g_3, \alpha_3, \beta_3$ are positive parameters with $0 < \alpha_3 < 1$ and $\beta_3 > 1$. According to Lemma 4, if $s_2 = 0$, z converges time-synchronously within $T_3 \leqslant 2^{\frac{1-\alpha_3}{2}}/(p_3(1-\alpha_3)) + 2^{\frac{1-\beta_3}{2}}(g_3(\beta_3-1))$.

In order to drive the sliding mode surface s_2 to zero and make z converge time-synchronously, the control input u is designed based on s_2,

$$u = u_1 + u_2, \tag{62}$$

$$\begin{aligned} u_1 = &- \left(A_{21}x_1 + A_{22}x_2 + p_3\mathrm{sig}_\mathrm{n}^{\alpha_3}(z) + g_3\mathrm{sig}_\mathrm{n}^{\beta_3}(z)\right) - B_{1,0}^{\dagger}\left(A_{11}'' + \varphi(v_1)\right)\left(\sum_{i=1}^{r} A_{1,i}'' v_i + B_{1,0}x_2\right) \\ &- B_{1,0}^{\dagger}\left(\Upsilon_3\mathrm{sign}_\mathrm{n}(s_1) + p_2\mathrm{sig}_\mathrm{n}^{\alpha_2}(s_1) + g_2\mathrm{sig}_\mathrm{n}^{\beta_2}(s_1)\right) - B_{1,0}^{\dagger}\sum_{i=2}^{r} A_{1,i}''\left(\bar{A}_i v_i + B_{i,i-1}' v_{i-1}\right), \end{aligned} \tag{63}$$

$$\dot{u}_2 = -\Upsilon_4\mathrm{sign}_\mathrm{n}(s_2) - \left(p_4\mathrm{sig}_\mathrm{n}^{\alpha_4}(s_2) + g_4\mathrm{sig}_\mathrm{n}^{\beta_4}(s_2)\right), \tag{64}$$

$$\begin{aligned} \Upsilon_4 = &\left\|B_{1,0}^{\dagger}\left(A_{11}''+\varphi\left(v_1\right)\right)B_{1,0}\right\|\left(\kappa_3\left\|x\right\|+\vartheta_3\right)+\kappa_2\|u_1\|+\vartheta_2 \\ &+\left\|B_{1,0}^{\dagger}\dot{\varphi}\left(v_1\right)B_{1,0}\right\|\left\|\eta_3\|x\|+h_3\right\|+\kappa_2\left\|\int_0^t \dot{u}_2\mathrm{d}t\right\|, \end{aligned} \tag{65}$$

where $p_4, g_4, \alpha_4, \beta_4$ are positive parameters with $0 < \alpha_4 < 1$ and $\beta_4 > 1$. The function $\varphi(v_1)$ is

$$\varphi\left(v_1\right) = p_1(\alpha_1 - 1)\|v_1\|^{\alpha_1-3}v_1v_1^\mathrm{T} + p_1\|v_1\|^{\alpha_1-1}I_{n-m} + g_1(\beta_1-1)\|v_1\|^{\beta_1-3}v_1v_1^\mathrm{T} + g_1\|v_1\|^{\beta_1-1}I_{n-m}. \tag{66}$$

The controller (62) is quasi-continuous and should be understood in the Filippov sense [34].

Theorem 2. Considering the state-dimension-dominant MIMO system (51), under Assumptions 1, 3, and 4, using the control input (62) and the virtual control signal (53), the tracking error z and the output $y = v$ will achieve semi-fixed-time-synchronized convergence. Specifically, z and v_1 will reach the sliding mode surfaces $s_2 = 0$ and $s_1 = 0$ in fixed-time, then move along these terminal sliding surfaces, and finally converge to their equilibrium time-synchronously within a fixed time interval.

Proof. Firstly, let us show that the tracking error z reaches the sliding mode surface $s_2 = 0$ in a fixed time. Substituting $z = x_2 - \phi$ into (61), the sliding mode surface s_2 becomes

$$\begin{aligned} s_2 =& \dot{x}_2 - \dot{\phi} + p_3\mathrm{sig}_\mathrm{n}^{\alpha_3}(z) + g_3\mathrm{sig}_\mathrm{n}^{\beta_3}(z) \\ =& A_{21}x_1 + A_{22}x_2 + u + d_2 + p_3\mathrm{sig}_\mathrm{n}^{\alpha_3}(z) + g_3\mathrm{sig}_\mathrm{n}^{\beta_3}(z) + B_{1,0}^{\dagger}(\Upsilon_3(x)\mathrm{sign}_\mathrm{n}(s_1) + p_2\mathrm{sig}_\mathrm{n}^{\alpha_2}(s_1) + g_2\mathrm{sig}_\mathrm{n}^{\beta_2}(s_1)) \\ &+ B_{1,0}^{\dagger}\frac{\mathrm{d}}{\mathrm{d}t}\left(\sum_{i=1}^{r} A_{1,i}'' v_i + p_1\mathrm{sig}_\mathrm{n}^{\alpha_1}(v_1) + g_1\mathrm{sig}_\mathrm{n}^{\beta_1}(v_1)\right) \\ =& A_{21}x_1 + A_{22}x_2 + u + d_2 + p_3\mathrm{sig}_\mathrm{n}^{\alpha_3}(z) + g_3\mathrm{sig}_\mathrm{n}^{\beta_3}(z) + B_{1,0}^{\dagger}\left(\Upsilon_3(x)\mathrm{sign}_\mathrm{n}(s_1) + p_2\mathrm{sig}_\mathrm{n}^{\alpha_2}(s_1) + g_2\mathrm{sig}_\mathrm{n}^{\beta_2}(s_1)\right) \\ &+ B_{1,0}^{\dagger}\left(A_{11}'' + \varphi(v_1)\right)\left(\sum_{i=1}^{r} A_{1,i}'' v_i + B_{1,0}x_2\right) + B_{1,0}^{\dagger}\sum_{i=2}^{r} A_{1,i}''\left(\bar{A}_i v_i + B_{i,i-1}' v_{i-1}\right) \\ &+ B_{1,0}^{\dagger}\left(A_{11}'' + \varphi(v_1)\right)B_{1,0}\omega. \end{aligned} \tag{67}$$

Under the control input (62), s_2 and its derivative are formulated as

$$\begin{aligned} s_2 &= u_2 + d_2 + B_{1,0}^{\dagger}\left(A_{11}'' + \varphi(v_1)\right)B_{1,0}\omega, \\ \dot{s}_2 &= \dot{u}_2 + \dot{d}_2 + B_{1,0}^{\dagger}\left(A_{11}'' + \varphi(v_1)\right)B_{1,0}\dot{\omega} + B_{1,0}^{\dagger}\dot{\varphi}(v_1)B_{1,0}\omega. \end{aligned} \tag{68}$$

Considering a Lyapunov candidate $V_2 = \frac{1}{2}s_2^\mathrm{T}s_2$, it has the following derivative:

$$\dot{V}_2 = s_2^\mathrm{T}\dot{s}_2 \leqslant s_2^\mathrm{T}\dot{u}_2 + \|s_2\|\left(\kappa_2\|u\| + \vartheta_2\right) + \|s_2\|\|B_{1,0}^{\dagger}\left(A_{11}'' + \varphi(v_1)\right)B_{1,0}\|(\kappa_3\left\|x\right\| + \vartheta_3)$$

$$+ \|s_2\|\|B_{1,0}^{\dagger}\dot{\varphi}(v_1)B_{1,0}\|(\eta_3\|x\| + h_3). \tag{69}$$

Substituting (62) into the above equation and recalling the formulation of $\mathrm{sig}_{\mathrm{n}}^{\alpha}(x)$, we have

$$\begin{aligned}\dot{V}_2 \leqslant & - s_2^{\mathrm{T}}\left(\Upsilon_4\mathrm{sign}_{\mathrm{n}}(s_2) + p_4\mathrm{sig}_{\mathrm{n}}^{\alpha_4}(s_2) + g_4\mathrm{sig}_{\mathrm{n}}^{\beta_4}(s_2)\right) + \kappa_2\|s_2\|\left(\|u_1\| + \|u_2\|\right) + \|s_2\|\vartheta_2 \\ & + \|s_2\|\|B_{1,0}^{\dagger}\left(A_{11}'' + \varphi(v_1)\right)B_{1,0}\|(\kappa_3\|x\| + \vartheta_3) + \|s_2\|\|B_{1,0}^{\dagger}\dot{\varphi}(v_1)B_{1,0}\|(\eta_3\|x\| + h_3) \\ \leqslant & - p_4\mathrm{sig}_{\mathrm{n}}^{\alpha_4}(s_2) - g_4\mathrm{sig}_{\mathrm{n}}^{\beta_4}(s_2) = -p_4\|s_2\|^{\alpha_4+1} - g_4\|s_2\|^{\beta_4+1} \\ \leqslant & - 2^{\frac{\alpha_4+1}{2}}p_4V_2^{\frac{\alpha_4+1}{2}} - 2^{\frac{\alpha_4+1}{2}}g_4V_2^{\frac{\beta_4+1}{2}},\end{aligned} \tag{70}$$

which is fixed-time stable according to Lemma 1, and the settling time for the convergence of s_2 is

$$T_4 \leqslant 2^{\frac{1-\alpha_4}{2}}/[p_4(1-\alpha_4)] + 2^{\frac{1-\beta_4}{2}}/[g_4(\beta_4-1)]. \tag{71}$$

After s_2 converges to zero within T_4, the tracking error z moves along the sliding mode surface $s_2 = 0$ and converges to zero time-synchronously within T_3. Then, $z = \dot{z} = 0$, the sliding mode surface s_1 converges to zero within a fixed time interval T_2 according to Lemma 5. As $s_1 = 0$, the system output v_1 converges to zero time-synchronously within T_1. The bound of the setting time for the whole process can be formulated as $T_{\mathrm{idd}} \leqslant T_1 + T_2 + T_3 + T_4$, thus completing the proof.

5 Comparative simulations

In this section, we validate the proposed method by comparative experiments. Since the unique feature of the proposed method is the time-synchronization property introduced by the norm-normalized sign function, the proposed method is compared with a conventional fixed-time controller which has the same structure as the proposed method except for the sign function.

5.1 Verification on an input-dimension-dominant system

In the input-dimension-dominant case, the proposed controller is compared with a fixed-time controller with the following formulation:

$$\bar{u} = \bar{u}_1 + \bar{u}_2, \tag{72}$$

$$\begin{aligned}\bar{u}_1 = & - \left(A_{21}x_1 + A_{22}x_2 + p_3\mathrm{sig}_{\mathrm{c}}^{\alpha_3}(z) + g_3\mathrm{sig}_{\mathrm{c}}^{\beta_3}(z)\right) - A_{12}^{\dagger}\left(\Upsilon_1(x)\mathrm{sign}_{\mathrm{c}}(\bar{s}_1) + p_2\mathrm{sig}_{\mathrm{c}}^{\alpha_2}(\bar{s}_1) + g_2\mathrm{sig}_{\mathrm{c}}^{\beta_2}(\bar{s}_1)\right) \\ & - A_{12}^{\dagger}\left(A_{11} + \bar{\varphi}(x_1)\right)\left(A_{11}x_1 + A_{12}x_2\right),\end{aligned} \tag{73}$$

$$\dot{\bar{u}}_2 = -\Upsilon_2(x,\bar{u})\mathrm{sign}_{\mathrm{c}}(\bar{s}_2) - p_4\mathrm{sig}_{\mathrm{c}}^{\alpha_4}(\bar{s}_2) - g_4\mathrm{sig}_{\mathrm{c}}^{\beta_4}(\bar{s}_2), \tag{74}$$

the following modified sliding-mode surfaces $\bar{s}_1$ and $\bar{s}_2$:

$$\bar{s}_1 = \dot{x}_1 + p_1\mathrm{sig}_{\mathrm{c}}^{\alpha_1}(x_1) + g_1\mathrm{sig}_{\mathrm{c}}^{\beta_1}(x_1),\ \bar{s}_2 = \dot{z} + p_3\mathrm{sig}_{\mathrm{c}}^{\alpha_3}(z) + g_3\mathrm{sig}_{\mathrm{c}}^{\beta_3}(z), \tag{75}$$

and the following $\bar{\varphi}(x_1)$:

$$\bar{\varphi}(x_1) = p_1\alpha_1\mathrm{sig}_{\mathrm{c}}^{\alpha_1-1}(x_1) + g_1\beta_1\mathrm{sig}_{\mathrm{c}}^{\beta_1-1}(x_1). \tag{76}$$

It can be observed that the controller (72) has the same structure and parameters as controller (26) except for three aspects: the different sign functions (4)–(6) and (7) and (8), the sliding-mode surfaces s_1, s_2 and $\bar{s}_1$, $\bar{s}_2$ which are based on different sign functions, and the different functions $\varphi(x_1)$ and $\bar{\varphi}(x_1)$. Similarly, the desired virtual velocity $\bar{\phi}(\bar{s}_1) = \bar{\phi}_1 + \bar{\phi}_2(\bar{s}_1)$ has the same structure and parameters as in (17) except for the sign functions and sliding-mode surfaces; thus the detailed formulation of $\bar{\phi}(\bar{s}_1)$ is omitted here.

Remark 6. The classical sign function $\mathrm{sig}_{\mathrm{c}}^{\alpha}(x)$ calculates the sign of every state element separately, whereas in the proposed method, the control input is calculated by $\mathrm{sig}_{\mathrm{n}}^{\alpha}(x)$ which regards the state vector as a whole and cooperates each state element with each other, extending the scalar formulation to the multivariable situation. Due to the difference between $\mathrm{sig}_{\mathrm{c}}^{\alpha}(x)$ and $\mathrm{sig}_{\mathrm{n}}^{\alpha}(x)$, the relevant procedures for the controller design and the system analysis differ from the existing literature and consequently lead to the time-synchronized property of the system.

Table 1 Parameters and initial values

Parameter	Value	Parameter	Value	Parameter	Value	Parameter	Value
α_1	0.6	p_1	1	ς_1	0.1	ς_2	0.1
α_2	0.6	p_2	1	κ_1	1	κ_2	1
α_3	0.6	p_3	1	η_1	1	η_2	1
α_4	0.6	p_4	1	ϑ_1	0.2	ϑ_2	0.2
β_1	1.1	g_1	0.1	h_1	0.2	h_2	0.2
β_2	1.1	g_2	0.1	x_{o1}	1	x_{o2}	-3
β_3	1.1	g_3	0.1	x_{o3}	-3	x_{o4}	2
β_4	1.1	g_4	0.1				

In order to demonstrate the merits of the proposed method in the input-dimension-dominant case, the vertical take-off and landing aircraft is used for a comparative experiment between controller (26) and controller (72). The dynamics of this aircraft are complex and nonlinear with varying parameters, whereas it is linearized and can be formulated as

$$x_{\mathrm{o}} = A_{\mathrm{o}}x_{\mathrm{o}} + b_{\mathrm{o}}u + d_{\mathrm{o}}(t, x_{\mathrm{o}}, u), \tag{77}$$

where subscript 'o' stands for the original system, $u = [u_1, u_2]$ is the two-dimensional control input with the collective pitch u_1 and the longitudinal cyclic pitch u_2, $x_{\mathrm{o}} = [x_{\mathrm{o}1}, x_{\mathrm{o}2}, x_{\mathrm{o}3}, x_{\mathrm{o}4}]$ is the state vector with the horizontal velocity $x_{\mathrm{o}1}$, the vertical velocity $x_{\mathrm{o}2}$, the pitch rate $x_{\mathrm{o}3}$ and the pitch angle $x_{\mathrm{o}4}$. The detailed value of system matrices A, B, and the disturbance vector can be found in [37].

Let $\bar{x}_{\mathrm{o}} = [x_{\mathrm{o}3}, x_{\mathrm{o}4}, x_{\mathrm{o}1}, x_{\mathrm{o}2}]$. The transformation matrix and the system disturbance take the value of

$$T = \begin{bmatrix} 1.000 & 0 & -9.511 & 0.371 \\ 0 & 1.000 & 0 & 0 \\ 0 & 0 & -2.778 & -0.064 \\ 0 & 0 & -1.297 & -0.162 \end{bmatrix}, \quad d_{\mathrm{o}}(t, x_{\mathrm{o}}, u) = \begin{bmatrix} (0.1x_{\mathrm{o}3} + 0.7x_{\mathrm{o}4})\sin(0.1x_{\mathrm{o}2}) \\ -0.3x_{\mathrm{o}4}\cos(0.3x_{\mathrm{o}4}t) \\ -2x_{\mathrm{o}1} - 0.3x_{\mathrm{o}2} \\ (0.2x_{\mathrm{o}1} + 0.4x_{\mathrm{o}4})\sin(0.4x_{\mathrm{o}3}) \end{bmatrix}. \tag{78}$$

From matrix T, we can achieve the transformed system state $x = T\bar{x}_{\mathrm{o}} = [x_1^{\mathrm{T}}, x_2^{\mathrm{T}}]^{\mathrm{T}}$ with $x_1 \in \mathbb{R}^{2\times 1}, x_2 \in \mathbb{R}^{2\times 1}$. The transformed system is formulated in (3) with $[d_1^{\mathrm{T}}, d_2^{\mathrm{T}}] = Td_{\mathrm{o}}$. The transformed state matrices are

$$A_{11} = \begin{bmatrix} -0.8849 & 4.2613 \\ 1 & 0 \end{bmatrix}, \; A_{12} = \begin{bmatrix} 3.7423 & -1.8857 \\ -5.520 & 4.4900 \end{bmatrix}, \; A_{21} = \begin{bmatrix} -0.0524 & 1.5244 \\ -0.0248 & 1.2413 \end{bmatrix}, \; A_{22} = \begin{bmatrix} 0.2094 & -0.1404 \\ 0.5738 & -1.0781 \end{bmatrix}. \tag{79}$$

The same parameters and initial state values are adopted for both controllers as listed in Table 1.

Since the general system is transformed to the formulation of (3), we first analyze the system state of the transformed system where $x = T\bar{x}_{\mathrm{o}}$. The transformed state x under the proposed controller is illustrated in Figure 1(a), where every dimension of x converges simultaneously at $t = 6.25$ s. Even if we zoom the figure at the magnitude of 10^{-3}, the convergence rate is well-controlled by (26) under disturbances and the time-synchronization property is shown clearly in the subfigure. The transformed states generated by the conventional fixed-time controller (72) are plotted in Figure 1(b), where different state elements converge to zero at separate time instants. The transformed state x_{12} converges firstly at $t = 4.94$ s, whereas other state elements reach the origin at $t = 6.88$ s. One may doubt that x_{11}, x_{21} and x_{22} can still converge at the same time. However, this phenomenon is generated by the inherent coupled property of the system instead of the controller.

Despite the transformed system, the states of the original system have different performances under (26) and (72), which are illustrated in Figures 2(a) and (b), respectively. In Figure 2(a), the state elements converge to the origin at $t = 6.25$ s simultaneously under the proposed controller, whereas they converge at $t = 4.94$ s and $t = 6.88$ s separately under the compared controller. The converging time instants can be figured out clearly in the enlarged subfigures.

The reason for the time synchronization under (26) and asynchronous convergence under (72) can be attributed to the different designs of sliding mode manifolds. The s_1 in (15) and the s_2 in (24) are

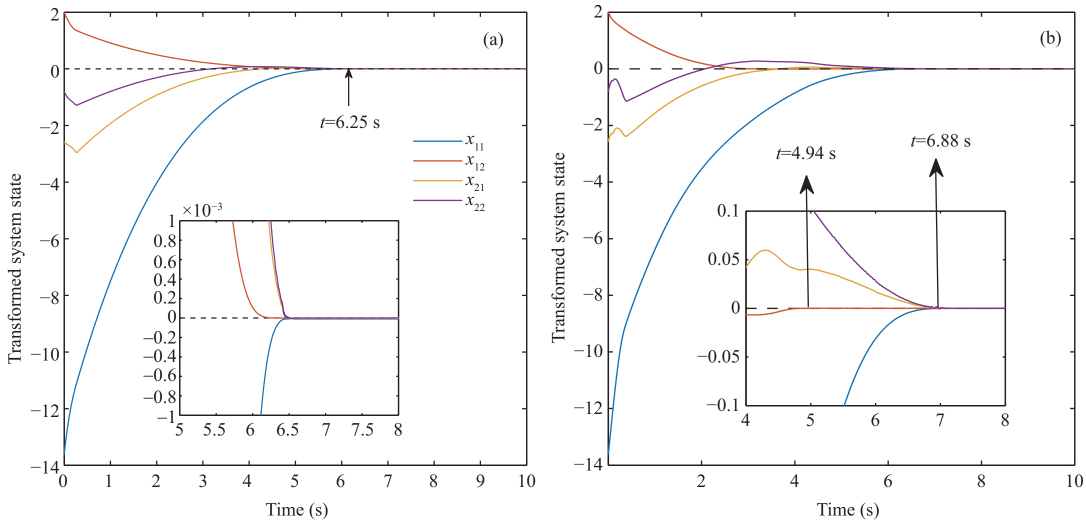

Figure 1 (Color online) Transformed state x by using (a) the time-synchronized controller in (26) and (b) the compared controller $\bar{u}$ in (72).

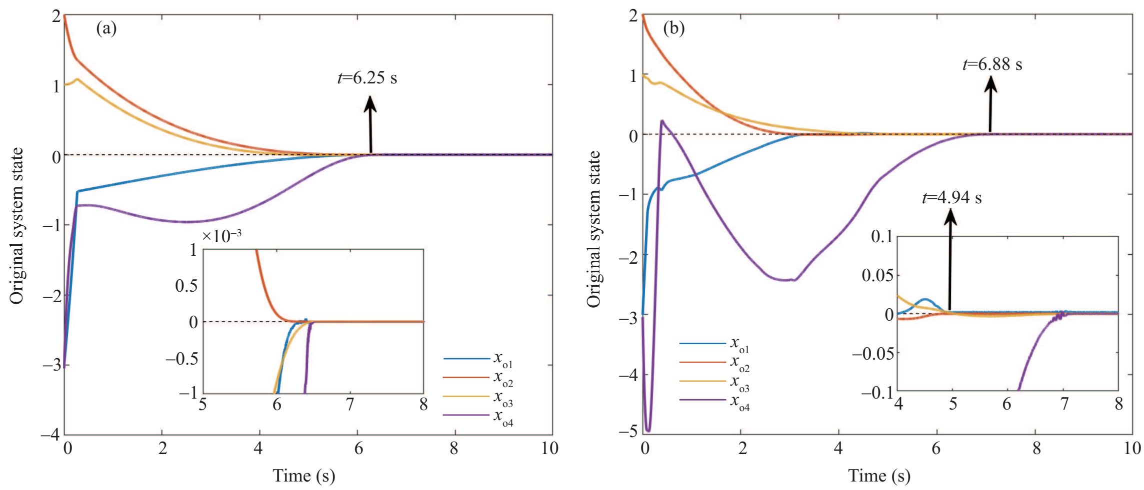

Figure 2 (Color online) Original state x_o by using (a) the time-synchronized controller (26) and (b) the compared controller $\bar{u}_1$.

designed based on the norm-normalized sign function, which cooperates multiple dimensions of the system state and keeps x_{11} and x_{12} ratio persistent. The ratio of x_{11} and x_{12} is illustrated in Figure 3, where a constant ratio is generated after a while under (26) and a changing ratio is generated by (72). The terminal sliding manifolds $\bar{s}_1$ and $\bar{s}_2$ are used for the compared fixed-time controller, where the classical sign function is adopted that deals with different dimensions separately, leading to the changing state ratios and sequential converging time instants.

The control inputs of the two controllers are demonstrated in Figure 3, where both control inputs are relatively large at the beginning and become very small when the system states reach the sliding-mode surfaces $s_1 = s_2 = 0$. The energy consumed by both controllers is also calculated and illustrated in Figure 3, where $E(t) = \sum_{i=1,2} \int_{\tau=0}^{t} u_i^2(\tau)\mathrm{d}\tau$. It can be observed that most of the energy is consumed at the first stage by driving the states to the sliding-mode surfaces. The proposed method is 20% less energy-consuming than the compared controller due to the time-synchronized property.

The rationale for the energy-saving performance can be figured out in Figure 4, where the state trajectory is plotted for both controllers. The state trajectory generated by the proposed controller (26) is illustrated as the blue line, which is a curve in the beginning when $s_1 \neq 0$ and becomes a straight line when $s_1 = 0$ after some time. A certain amount of control energy is consumed at the beginning whereas little control energy is needed when $s_1 = 0$. In contrast, the state trajectory generated by the compared controller (72) appears as a curve in the whole process, which consumes more energy. Moreover, the blue state trajectory under (26) is much shorter than the red one generated by (72).

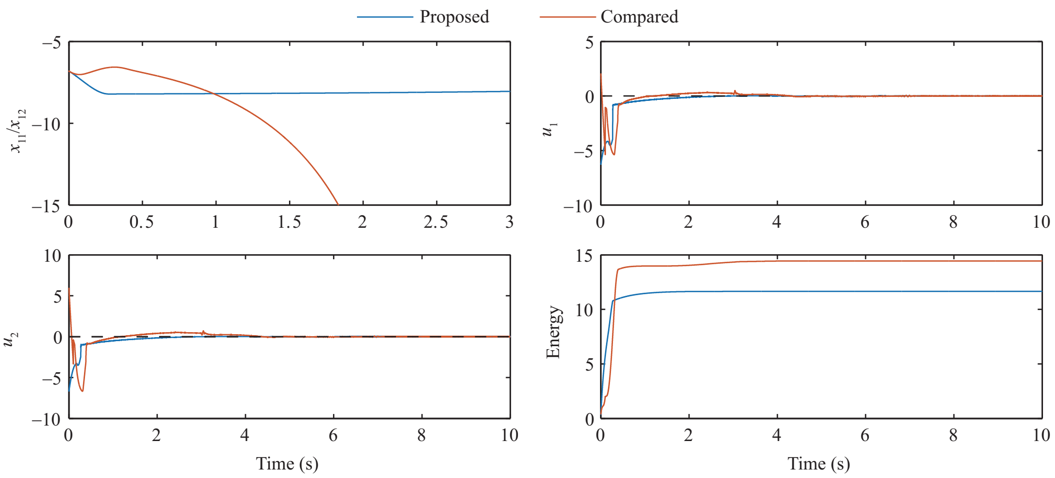

Figure 3 (Color online) The state ratio x_{11}/x_{12}, control inputs u_1 and u_2, and the energy consumed under controllers (26) and (72).

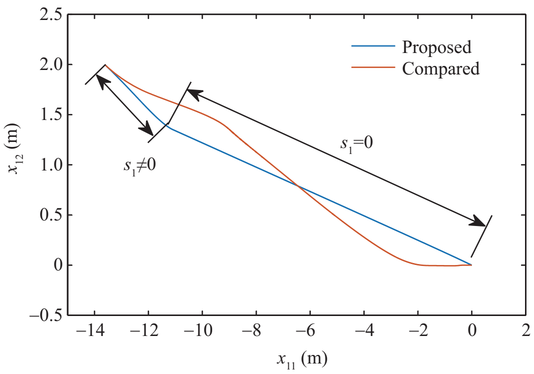

Figure 4 (Color online) The state trajectories of x_1 under different controllers.

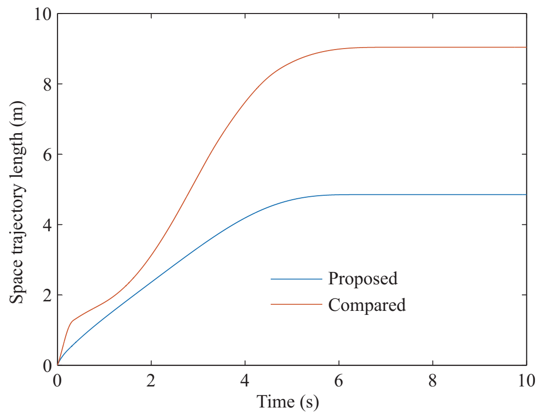

Figure 5 (Color online) The space trajectory length of the aircraft in (77) and $\bar{u}_1$ under different controllers.

Besides the state trajectories, the actual travel length can be explored since we use the practical aircraft as the simulation example. In Figure 5, the travel length of the aircraft is illustrated. It is calculated by integrating the 2-D speed, namely $d(t) = \int_{\tau=0}^{t} \sqrt{x_{o1}^2(\tau) + x_{o2}^2(\tau)}\mathrm{d}\tau$, where x_{o1} and x_{o2} are the horizontal velocity and the vertical velocity of the aircraft, respectively. Before the aircraft stops at the space, it travels 4.85 m under (26), which is much less than the 9.04 m generated by (72). This further showcases the merit of the proposed method.

5.2 Verification on a state-dimension-dominant system

In this subsection, a less complicated example is used to verify the fixed-time-synchronized control method for the state-dimension-dominant system (51), which is set as 5 state dimensions and 2 input dimensions.

The system matrices are $A''_{11} = \mathrm{diag}(-0.2, -2), B_{1,0} = 2I_2, A_{22} = \mathrm{diag}(-1, -0.5)$, $A''_{12} = \mathbf{0} \in \mathbb{R}^{1\times 2}$, $A_{21} = \mathbf{0} \in \mathbb{R}^{3\times 2}$, $\bar{A}_1 = [0, 1]$ and $B'_{2,1} = -1$. The disturbances are formulated as

$$d_2 = \begin{bmatrix} \sin(2x_{21})(0.2z_2 + 0.6x_{22}) \\ 0.5x_{22} + (z_{11} + 0.3z12)\cos(0.5x_{22}) \end{bmatrix}, \quad \omega = \begin{bmatrix} -0.4z_{11}\cos(0.5x_{21}) \\ -x_{22} + z_{12} \end{bmatrix}. \tag{80}$$

The proposed semi-fixed-time-synchronized controller (62) is modified to be

$$\bar{u} = \bar{u}_1 + \bar{u}_2, \tag{81}$$

$$\bar{u}_1 = -\left(A_{21}x_1 + A_{22}x_2 + p_3\mathrm{sig}_{\mathrm{c}}^{\alpha_3}(z) + g_3\mathrm{sig}_{\mathrm{c}}^{\beta_3}(z)\right) - B_{1,0}^{\dagger}\left(A''_{11} + \varphi(v_1)\right)\left(\sum_{i=1}^{r} A''_{1,i}v_i + B_{1,0}x_2\right)$$

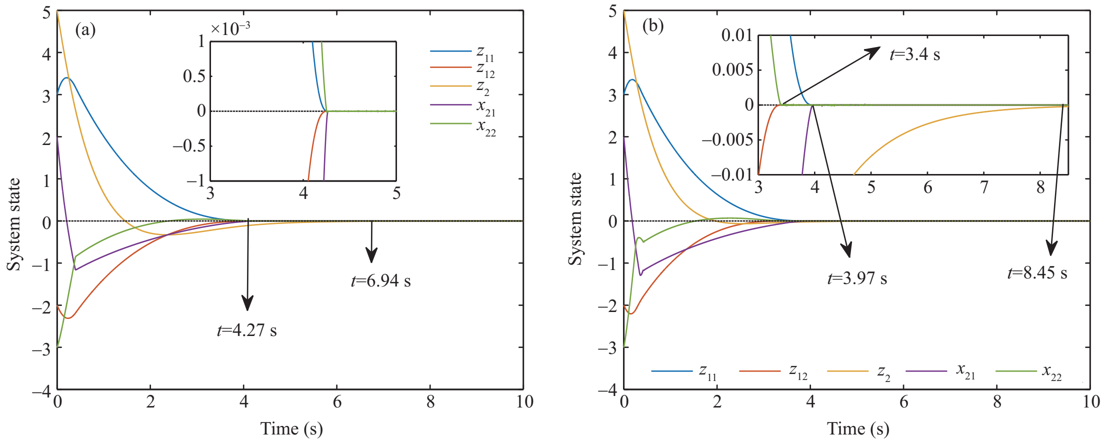

Figure 6 (Color online) System state x by using (a) the proposed controller (62) and (b) the compared controller (81).

$$- B_{1,0}^{\dagger}\left(\Upsilon_3 \mathrm{sign_c}(\bar{s}_1) + p_2 \mathrm{sig}_{\mathrm{c}}^{\alpha_2}(\bar{s}_1) + g_2 \mathrm{sig}_{\mathrm{c}}^{\beta_2}(\bar{s}_1)\right) - B_{1,0}^{\dagger} \sum_{i=2}^{r} A''_{1,i}\left(\bar{A}_i v_i + B'_{i,i-1} v_{i-1}\right), \tag{82}$$

$$\dot{\bar{u}}_2 = - \Upsilon_4(x,\bar{u}) \mathrm{sign_c}(\bar{s}_2) - p_4 \mathrm{sig}_{\mathrm{c}}^{\alpha_4}(\bar{s}_2) - g_4 \mathrm{sig}_{\mathrm{c}}^{\beta_4}(\bar{s}_2), \tag{83}$$

where the function $\varphi(v_1)$ is the same as (76) with variable v_1 and the sliding-mode manifolds are reformulated as

$$\bar{s}_1 = \dot{v}_1 + p_1 \mathrm{sig}_{\mathrm{c}}^{\alpha_1}(v_1) + g_1 \mathrm{sig}_{\mathrm{c}}^{\beta_1}(v_1),\ \ \bar{s}_2 = \dot{z} + p_3 \mathrm{sig}_{\mathrm{c}}^{\alpha_3}(z) + g_3 \mathrm{sig}_{\mathrm{c}}^{\beta_3}(z). \tag{84}$$

Similar to Subsection 5.1, controller (81) has the same structure and parameters as controller (62) except for the different sign functions, the sliding-mode surfaces based on different sign functions, and the functions $\varphi(v_1)$ and $\bar{\varphi}(v_1)$. The desired virtual velocity $\bar{\phi}(\bar{s}_1) = \bar{\phi}_1 + \bar{\phi}_2(\bar{s}_1)$ has the same structure and parameters as in (53) except for the sign functions and the sliding-mode surfaces.

The same control parameters are adopted for both the proposed semi-fixed-time-synchronized controller (62) and the compared fixed-time controller (81), which are set to be the same as in Subsection 5.1 and are shown in Table 1. The initial values of the original system states are $z_1 = [3,-2]^{\mathrm{T}}, z_2 = 5; x_2 = [2,-3]^{\mathrm{T}}$.

Figure 6(a) shows the state of the system (51) under the proposed controller (62), where z_{11}, z_{12}, x_{21} and x_{22} converge simultaneously at $t = 4.27$ s whereas z_2 reaches zero at $t = 6.94$ s. It is called "semi-time-synchronized" control because only parts of the output dimensions, namely z_{11} and z_{12}, converge time-synchronously. The other part of the output dimensions, z_2, reaches the origin at a different time instant since the control input is not powerful enough to drive all the state elements to the origin simultaneously. In this case, the sliding mode manifolds s_1 in (52) and s_2 in (61) are designed for z_1 and x_2, respectively, the two dimensions of z_1 are expected to reach the origin simultaneously and so do the dimensions of x_2, whereas z_1 and x_2 are not designed to converge time-synchronously. They converge simultaneously simply due to the inherent coupling of the system. The time-synchronization property is shown clearly in the subfigure, where the plots are zoomed at the magnitude of 10^{-3}. Figure 6(b) is illustrated as a comparison, which is generated by the compared controller (81). In Figure 6(b), z_{11} and x_{21} converge at $t = 3.97$ s, z_{12} and x_{22} reach zero at $t = 3.4$ s, and z_2 arrives at the origin at $t = 8.45$s. The three dimensions of the output, z_{11}, z_{12} and z_2, converge totally time-asynchronously.

The output ratio, the control input, and the energy consumed by both controllers (62) and (81) are illustrated in Figure 7. Only the ratio of z_{11}/z_{12} is plotted because the sliding-mode surface s_1 in (52) is designed for the fixed-time-synchronized of z_1, and z_2 converges at a different time instant. The ratio of z_{11}/z_{12} is persistent in the stabilizing process under the proposed controller (62) whereas it keeps varying under the compared controller (81). This results in the synchronized/asynchronous converging time of the two controllers. The control energy is calculated as $E(t) = \sum_{i=1,2} \int_{\tau=0}^{t} u_i^2(\tau) \mathrm{d}\tau$. The proposed method saves about 1/3 control energy with respect to the conventional fixed-time controller (81).

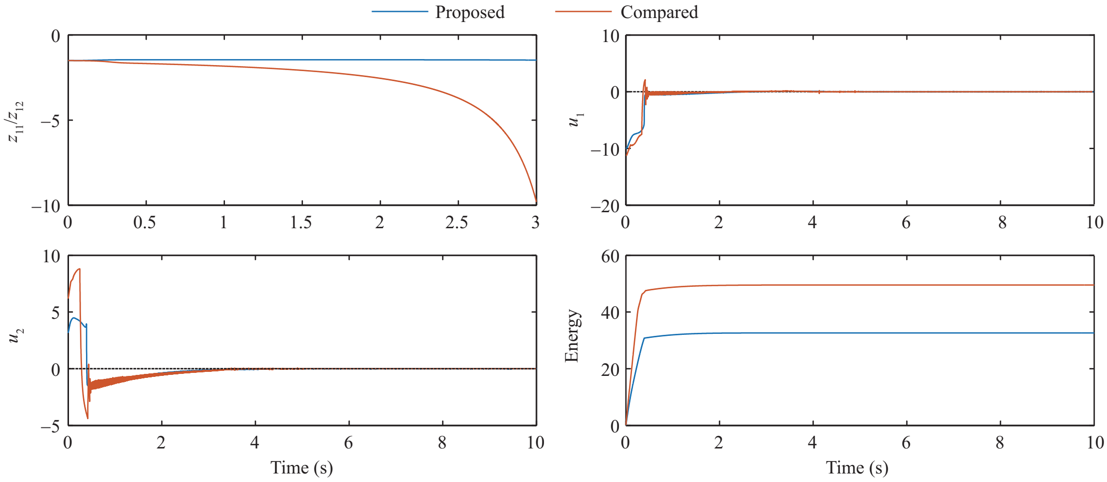

Figure 7 (Color online) The state ratio z_{11}/z_{12}, control inputs u_1 and u_2, and the energy consumed under controllers (62) and (81).

6 Conclusion

This study considers the fixed-time-synchronized control of perturbed MIMO systems. A general MIMO system is divided into input-dimension-dominant and state-dimension-dominant cases, which are defined according to the capability of achieving time-synchronized convergence. A fixed-time-synchronized terminal sliding-mode surface is presented as the foundation of the proposed method, based on which the (semi-) fixed-time-synchronized controllers are designed for input-dimension-dominant and state-dimension-dominant cases. Matched disturbances that appear inside the control channel and unmatched disturbances that appear outside the control channel are both considered and compensated by a super-twisting observer embedded in the controller. Analysis and discussions on system stability and time-synchronized property are conducted. Compared with conventional controllers, the proposed method generates shorter state trajectories and consumes lower control energy, which is verified by simulations. The merits come from the time-synchronized property, which can be extended to some existing fixed-time controllers by certain modifications based on the inspiration of this study. In the future, the proposed control method will be improved to deal with more complicated practical problems, such as input saturation and reference signal variation, and its application will be explored in the rendezvous of multiple vehicles and the time-synchronized arrival of robot fingers.

Acknowledgements This work was supported by National Key Research and Development Program of China (Grant No. 2020YFB1313604), National Natural Science Foundation of China (Grant No. 62103028), and Natural Science Foundation of Zhejiang Province (Grant No. LGG22F030018).

References

1 Zuo Z Y, Song J W, Tian B L, et al. Robust fixed-time stabilization control of generic linear systems with mismatched disturbances. IEEE Trans Syst Man Cybern Syst, 2022, 52: 759–768
2 Haimo V T. Finite time controllers. SIAM J Ctrl and Optimiz, 1986, 4: 760–770
3 Bhat S P, Bernstein D S. Finite-time stability of continuous autonomous systems. SIAM J Control Optim, 2000, 38: 751–766
4 Polyakov A, Efimov D, Perruquetti W. Robust stabilization of MIMO systems in finite/fixed time. Int J Robust Nonlinear Control, 2016, 26: 69–90
5 Zhang L Y, Liu H, Tang D F, et al. Adaptive fixed-time fault-tolerant tracking control and its application for robot manipulators. IEEE Trans Ind Electron, 2021, 69: 2956–2966
6 Zhang L J, Xia Y Q, Shen G H, et al. Fixed-time attitude tracking control for spacecraft based on a fixed-time extended state observer. Sci China Inf Sci, 2021, 64: 212201
7 Hong H F, Wang H, Wang Z L, et al. Finite-time and fixed-time consensus problems for second-order multi-agent systems with reduced state information. Sci China Inf Sci, 2019, 62: 212201
8 Ning B D, Han Q L, Zuo Z Y, et al. Fixed-time and prescribed-time consensus control of multiagent systems and its applications: a survey of recent trends and methodologies. IEEE Trans Ind Inf, 2023, 19: 1121–1135
9 Chang S P, Wang Y J, Zuo Z Q. Fixed-time active disturbance rejection control and its application to wheeled mobile robots. IEEE Trans Syst Man Cybern Syst, 2020, 51: 7120–7130
10 Polyakov A. Nonlinear feedback design for fixed-time stabilization of linear control systems. IEEE Trans Automat Contr, 2012, 57: 2106–2110
11 Corradini M L, Cristofaro A. Nonsingular terminal sliding-mode control of nonlinear planar systems with global fixed-time stability guarantees. Automatica, 2018, 95: 561–565
12 Yan W, Liu Y C, Lan Q J, et al. Trajectory planning and low-chattering fixed-time nonsingular terminal sliding mode control for a dual-arm free-floating space robot. Robotica, 2022, 40: 625–645

13 Gutman S. Uncertain dynamical systems–a Lyapunov min-max approach. IEEE Trans Automat Contr, 1979, 24: 437–443
14 Nagesh I, Edwards C. A multivariable super-twisting sliding mode approach. Automatica, 2014, 50: 984–988
15 Yu D X, Chen C L P, Xu H. Fuzzy swarm control based on sliding-mode strategy with self-organized omnidirectional mobile robots system. IEEE Trans Syst Man Cybern Syst, 2022, 52: 2262–2274
16 Zhang L, Wei C Z, Wu R, et al. Fixed-time extended state observer based non-singular fast terminal sliding mode control for a VTVL reusable launch vehicle. Aerospace Sci Tech, 2018, 82–83: 70–79
17 Koval M C, Pollard N S, Srinivasa S S. Pre- and post-contact policy decomposition for planar contact manipulation under uncertainty. Int J Robotics Res, 2016, 35: 244–264
18 Rucco A, Sujit P B, Aguiar A P, et al. Optimal rendezvous trajectory for unmanned aerial-ground vehicles. IEEE Trans Aerosp Electron Syst, 2017, 54: 834–847
19 Jiang W, Li D, Ge S S. Micro flapping-wing vehicles formation control with attitude estimation. IEEE Trans Cybern, 2022, 52: 1035–1047
20 Miyata N, Ota J, Arai T, et al. Cooperative transport by multiple mobile robots in unknown static environments associated with real-time task assignment. IEEE Trans Robot Automat, 2002, 18: 769–780
21 Jeon I S, Lee J I, Tahk M J. Homing guidance law for cooperative attack of multiple missiles. J Guid Control Dyn, 2010, 33: 275–280
22 Li D Y, Ge S S, Lee T H. Simultaneous arrival to origin convergence: sliding-mode control through the norm-normalized sign function. IEEE Trans Automat Contr, 2022, 67: 1966–1972
23 Li D Y, Yu H Y, Tee K P, et al. On time-synchronized stability and control. IEEE Trans Syst Man Cybern Syst, 2022, 52: 2450–2463
24 Jin X. Adaptive fixed-time control for MIMO nonlinear systems with asymmetric output constraints using universal barrier functions. IEEE Trans Automat Contr, 2019, 64: 3046–3053
25 Shi S, Sun Y H, Hu Y L, et al. Robust fixed-time output-feedback control for linear systems without chattering: an exact uncertainty compensation method. Sci China Inf Sci, 2022, 65: 179201
26 Amrr S M, Banerjee A, Nabi M. Time-energy efficient finite time attitude tracking control of spacecraft using disturbance observer. IFAC-PapersOnLine, 2020, 53: 5964–5969
27 Utkin V, Guldner J, Ma S J. Sliding Mode Control in Electro-Mechanical Systems. Boca Raton: CRC Press, 1999
28 DeCarlo R A, Zak S H, Matthews G P. Variable structure control of nonlinear multivariable systems: a tutorial. Proc IEEE, 1998, 76: 212–232
29 Loukianov A G, Utkin V I. Time-varying linear system decomposed control. In: Proceedings of American Control Conference, 1998. 2884–2888
30 Hamayun M T, Edwards C, Alwi H. Design and analysis of an integral sliding mode fault-tolerant control scheme. IEEE Trans Automat Contr, 2012, 57: 1783–1789
31 Sanyal A K, Bohn J. Finite-time stabilisation of simple mechanical systems using continuous feedback. Int J Control, 2015, 88: 783–791
32 Basin M. Finite- and fixed-time convergent algorithms: Design and convergence time estimation. Annu Rev Control, 2019, 48: 209–221
33 Edwards C, Spurgeon S. Sliding Mode Control: Theory and Applications. Boca Raton: CRC Press, 1998
34 Filippov A F. Differential Equations With Discontinuous Righthand Sides: Control Systems. Dordrecht: Springer, 2013. 18
35 Feng Y, Zhou M H, Zheng X M, et al. Full-order terminal sliding-mode control of MIMO systems with unmatched uncertainties. J Frank Inst, 2018, 355: 653–674
36 Utkin V I, Drakunov S V, Izosimov D E, et al. A hierarchical principle of the control system decomposition based on motion separation. IFAC Proc Vol, 1984, 17: 1553–1558
37 Singh S N, Coelho A A R. Nonlinear control of mismatched uncertain linear systems and application to control of aircraft. J Dyn Syst Meas Control, 1984, 106: 203–210